DOI: https://doi.org/10.57233/ihcfs.046

ISBN: 978-978-68-07775

BOOK OF PROCEEDINGS

IHCFS – 2025 WEBSITE: fos.fugusau.edu.ng

1ST INTERNATIONAL HYBRID CONFERENCE OF FACULTY OF SCIENCE

(A PUBLICATION OF FACULTY OF SCIENCE, FEDERAL UNIVERSITY GUSAU, NIGERIA)

Velocity Slip Effect on Unsteady MHD Natural Convection Flow of Casson Fluid Incorporating Variable Suction, Thermal Radiation and Chemical Reaction Mechanisms

Farisa Muhammad[1], Emmanuel Omokhuale[1], Salisu Muhammad Muhammad[1] and Lawal Sa'adu[2]

[1]Department of Mathematical Sciences, Federal University Gusau, P. M. B. 1001, Zamfara State, Nigeria.

[2]Department of Physics, Federal University Gusau, P. M. B. 1001, Zamfara State, Nigeria.

Corresponding Author's Email: farisamuhammad02@gmail.com

ABSTRACT

Velocity slip effect on unsteady MHD natural convection flow of Casson fluid incorporating variable suction, thermal radiation and chemical reaction mechanisms has been examined. The governing equations are: continuity, momentum, energy and mass equations. The partial differential equations (PDEs) for the problem were transformed into ordinary differential equations (ODEs) and solved analytically using regular perturbation method where the velocity, temperature and concentration fields were gotten. The coefficients for skin-friction, rate of heat and mass transfer were derived from the solutions of velocity, temperature and concentration. The effect of physical parameters of interest on the velocity, temperature and concentration of the fluid were computed and presented graphically. In addition, the study contributes to a better understanding of the behaviour of non-Newtonian fluids under different thermal and concentration gradients and has practical implications in various industrial processes. The most significant conclusion of this work is that as Casson parameter and velocity slip increase, the velocity of the fluid becomes higher while a reverse trend is seen as thermal radiation and chemical reaction parameter are raised. Additionally, the thermal and mass boundary layers of the fluid rises due to decrease in thermal radiation and chemical reaction parameters.

Keywords: Casson fluid; Variable Suction; Thermal Radiation; Chemical Reaction; Velocity Slip.

Nomenclature

List of variable

Gr	Thermal Grashof Number
Gm	Mass Grashof Number
Pr	Prandtl Number
Kc	Chemical Reaction Parameter
M	Magnetic Parameter
R	Thermal Radiation Parameter
H	Heat Absorption Parameter
S	Suction parameter
K	Permeability Parameter
Q_r	Heat absorption flux
Sc	Schmidt Number
y^*	Dimensional coordinate perpendicular to the plate
C^*	Dimensional concentration of the fluid
T^*	Dimensional temperature of the fluid
u^*	Dimensional velocity of the fluid
u_c	Reference velocity (ms^{-1})
C_p	Specific heat at constant pressure $(JKg^{-1}K)$

DOI: https://doi.org/10.57233/ihcfs.046

ISBN: 978-978-68-07775

BOOK OF PROCEEDINGS

IHCFS – 2025 WEBSITE: fos.fugusau.edu.ng

D	Mass diffusivity $(m^2 s^{-1})$
T_m	Mean fluid temperature (K)
k_T	Thermal diffusion ratio
k^*	Mean absorption coefficient
g	Acceleration due to gravity (ms^{-1})
k_p	Thermal conductivity (W $K^{-1}m^{-1}$)
T_w^*	Temperature of fluid near to moving plate (K)
T_∞^*	Temperature of fluid near to stationary plate (K)
C_w^*	Concentration of fluid near to moving plate (mol m^{-3})
C_∞^*	Concentration of fluid near to the stationary plate (mol m^{-3})
Q_0	The heat generation constant
y^*	Dimensional coordinate perpendicular to the plate
C^*	Dimensional concentration of the fluid
T^*	Dimensional temperature of the fluid
u^*	Dimensional velocity of the fluid
u	Dimensionless velocity of the fluid
t^*	Dimensional time
t	Dimensionless time
Greek symbols	
β	Casson Parameter
ρ	Fluid Density
υ	Kinematic Viscosity
σ	Electric Conductivity of the Fluid (ms^{-1})
β_1	Coefficient of Volume Expansion for Mass Transfer $(m^3 kg^{-1})$
β	Thermal expansion coefficient (k^{-1})
μ	Dynamic viscosity (kg $m^{-1}s^{-1}$)
ε	Activation energy parameter
ξ	Dimensionless coordinate perpendicular to the plate
φ	Dimensionless concentration of the fluid
η	Dimensionless temperature of the fluid
γ	Slip parameter
Superscript	
*	Dimensional properties
Subscripts	
P	Plate
w	Wall condition
∞	Free stream condition

1.0 INTRODUCTION

The velocity slip effect on unsteady Magnetohydrodynamics (MHD) natural convection flow of a Casson fluid, a non-Newtonian fluid with yield stress, is a complex phenomenon studied to understand

DOI: https://doi.org/10.57233/ihcfs.046

ISBN: 978-978-68-07775

BOOK OF PROCEEDINGS

heat transfer and fluid motion in various applications. Casson fluids, used in many industries like biometrics and polymer production, exhibit unique flow properties due to their yield stress behavior. The inclusion of thermal slip, a boundary condition where fluid velocity differs from the wall velocity, significantly impacts heat transfer and fluid dynamics in these systems.

The phenomenon “slip” may take place on the stretching boundary when the liquid is in the form of suspensions such as, nanofluid, polymer solutions and foams. The non-adherence solid–fluid interface motion, also called velocity slip, is a hydrodynamic term that has been examined under some conditions (Wang and Ng, 2011). Mukhopadhyay (2013) presented a numerical study of nanofluid flow in the presence of velocity slip over an elongating tube. She found that slip reduces velocity but increases the temperature profile. This priceless information leads to improvement of flow model associated with slip conditions. Later, Hayat *et al*. (2014) used thermal slip along with velocity slip to discuss the heat and mass transfer performance over a vertical stretching tube. (Mishra and Kumar, 2020).

Moreso, natural convection is a prevalent occurrence in which convective flow is naturally established in a liquid body as a consequence of the formation of a pressure differential caused by a gradient of temperature. Natural convection occurs when a fluid close to a hot source absorbs heat, and as a result of thermal expansion, it becomes less dense and rises. In its location, a lighter or warmer liquid displaces the adjacent colder liquid. A current of convection is created as a result of heating this colder fluid once more and continuing the process. It has numerous uses, including temperature management, biological systems, and thermal energy preservation. The chilling of electrical and electronic parts, air conditioner elements, and equipment in the steel industry all benefit greatly from natural convection (Ragulkumar, *et al*. 2023). Natural convection in porous media in a highly nonlinear metaphysical engineering applications was demonstrated by Kadeethum *et al.* (2022).

The investigation of Magnetohydrodynamic (MHD) flow of non-Newtonian fluid in a porous medium has attracted the attentions of a various researchers. Obviously, it is owing to the reality that such phenomenon’s are predominantly establish in the optimization of solidification processes of metals and metal alloys, the geothermal sources examination and nuclear fuel debris treatment. However, non-Newtonian fluids are slight compare to Newtonian fluids. Certainly, the resulting equations of non-Newtonian fluids give highly non-linear differential equations which are generally difficult to solve. These equations add further complexities when MHD flows in a porous space have been taken into account. Sufficient applications for the MHD flows of Casson fluids in a porous medium are experienced in biological systems, irrigation problems, process of petroleum, heat-storage beds, textile, polymer composite and paper industries. Several researchers have been presented on different aspects of MHD flows of Casson fluid flows passing through a porous medium. Various examinations have been introduced on different parts of MHD non-Newtonian liquid streams going through a permeable medium (Rajakumar *et al*. 2020). The MHD convection flow of Casson fluid in micro-channels including porous material was discussed by Gireesha and Sindhu (2020).

In general, radiation effects on fluid flow include the effects caused by the transfer of thermal radiation on the heat transfer as well as the behavior of the fluid in the motion. Radiative heat transfer in a fluid flow implies that heat is not transferred only by conduction where the heat from the molecules of fluid is transmitted to other molecules or by convection where the heated fluid is transferred but also by electromagnetic waves. The added mode of

DOI: https://doi.org/10.57233/ihcfs.046

ISBN: 978-978-68-07775

heat transfer strongly modifies the temperature distribution within the fluid, in particular for high temperature environments or flows over heated boundaries. In many engineering and industrial applications, for example in nuclear reactors, combustion chambers, astrophysical flows or spacecraft thermal control, where radiation heat transfer can be more important than conduction or convection, radiation effects should not be disregarded. Radiation assists in the development of the boundary layer, determines thermal gradients of the fluid, and works together with the kinetic energy to determine thermal stability of the fluid. The correct design of radiation in liquids in motion makes it possible to use energy efficiently, to improve the cooling process, and to raise the energy stability limits of materials used in high-temperature conditions (Prakash et al., 2025).

Meanwhile, thermo chemical reactions involving fluids and masses are common in chemical engineering procedures involving moving plates. The synthesis of polymers, the production of ceramics or glassware, and the processing of food are among the many industrial applications of these processes, according to Joshna *et al*. (2022). The influence of chemical reactions and radiation absorption on unsteady MHD free convective flow was investigated by Ibrahim *et al*. (2008). By exposing a semi-infinite, vertically permeable moving plate to a heat source and suction, observers were able to see the flow. Chemical reaction effects on multi-phase heat transfer (MHFT) were studied by Agarwalla *et al*. (2018) in the context of a porous media, an inclined plate, thermal radiation, a heat source, and a variable plate velocity embedded in a porous medium.

Recently, Mahmood *et al.* (2025) provided an in-depth study of how mixed convective effects on concentration and temperature impact mass, heat, and non-Newtonian Casson fluid flow. In their study, they considered, a transverse magnetic field and vertical permeable stretched sheet affect the fluid. Furthermore, nonlinear thermal radiation, Brownian motion, thermophoresis, velocity slip, and temperature slip were examined.

Manthramurthy & Vempati (2025) examined the thermal and mass transfer properties of a magnetohydrodynamic Casson nanofluid flowing over a nonlinear porous stretching sheet subjected to a magnetic field. Their study considered chemical reactions, thermophoresis, non-uniform heat sources or sinks, and the Soret and Dufour effects. Consequently, their analysis incorporates various slip parameters and a convective boundary condition. The controlling nonlinear partial differential equations are turned into nonlinear ordinary differential equations via similarity transformations.

In this paper, motivated by the applications and phenomenon mentioned above, the effects of chemical reaction and thermal radiation on MHD natural convection flow of Casson fluid incorporating variable suction has been investigated. The flow was unsteady and constrained to the laminar domain to address the gap existing in literature. The governing equations for this consideration are solved using regular perturbation method. The effects of important physical parameters on temperature, concentration and velocity fields were plotted and presented graphically. The expressions for skin friction, rate of heat and mass transfer were deduced from the solutions of velocity, temperature and concentration.

2.0 MATHEMATICAL FORMULATION

We consider Casson fluid flow through a vertical channel. The flow being confined to y>0, where y is the coordinate measured in the normal direction to the plate. The fluid is assumed to be electrically conducting with a uniform magnetic field of strength (See Figure 2.1).

DOI: https://doi.org/10.57233/ihcfs.046

ISBN: 978-978-68-07775

BOOK OF PROCEEDINGS

IHCFS – 2025 WEBSITE: fos.fugusau.edu.ng

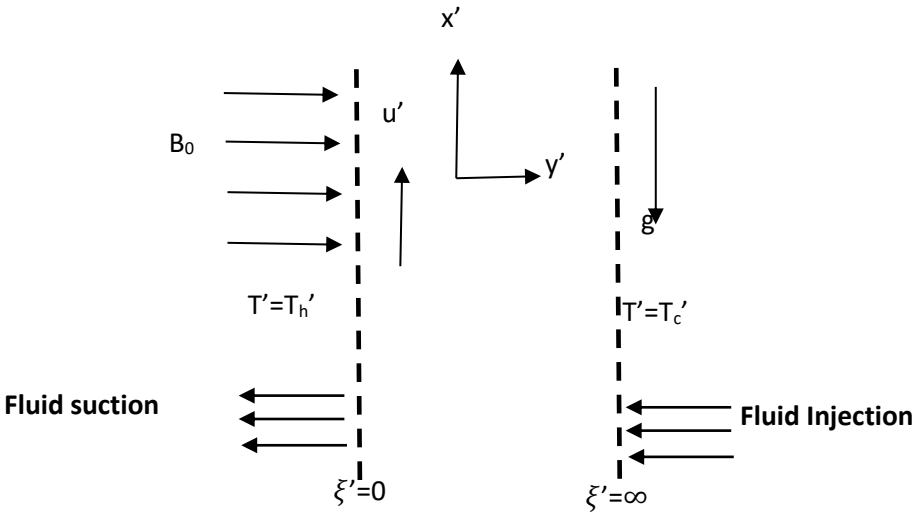

Figure 2.1: Schematic Diagram

Initially, the fluid is at the same temperature θ in a stationary condition with concentration level at all point.

The rheological equation or state of Cauchy stress tensor of Casson fluid is written as

$\tau=\tau_0+\mu\dot{\gamma}$

or

$$\tau_{ij}=\begin{cases}2\left(\mu_\beta+\frac{P_y}{\sqrt{2\pi}}\right)e_{ij}, & \pi>\pi_c\\ 2\left(\mu_\beta+\frac{P_y}{\sqrt{2\pi}}\right)e_{ij}, & \pi>\pi_c\end{cases}$$

where $\pi= e_{ij}$ and e_{ij} is the $(i,j)^{th}$ component of the deformation rate, π is the product of the component of deformation rate with itself. Also, π_c is a critical value of this product based on the non-Newtonian model, μ_β is plastic dynamic viscosity of the non-Newtonian fluid and P_y is yield stress fluid. The equations governed the unstudied boundary layer flow of the casson fluid are as follows:

$$\frac{\partial v}{\partial y}=0 \tag{1}$$

$$\rho\left[\frac{\partial u^*}{\partial t^*}+v\frac{\partial u^*}{\partial y^*}\right]=\mu\left(1+\frac{1}{\beta}\right)\frac{\partial^2 u^*}{\partial y^{*2}}-\delta\beta_0^2u^*+\rho g\beta\left(T^*-T_\infty^*\right)+\rho g\beta_1\left(C^*-C_\infty^*\right)-\left(1+\frac{1}{\beta}\right)\frac{\mu\phi}{K_p}u^* \tag{2}$$

$$\rho C_p\left[\frac{\partial T^*}{\partial t^*}+v\frac{\partial T^*}{\partial y^*}\right]=K_T\frac{\partial^2 T^*}{\partial y^{*2}}-\frac{\partial Qr}{\partial y^*}-Q_0\left(T^*-T_\infty^*\right) \tag{3}$$

$$\frac{\partial C^*}{\partial t^*}+v\frac{\partial C^*}{\partial y^*}=D\frac{\partial^2 C^*}{\partial y^{*2}}-K^*\left(C^*-C_\infty^*\right) \tag{4}$$

The initial and boundary conditions are as follows:

$t\le 0: u=0,\eta=T_\infty^*,\phi=C_\infty^*$ for all ξ

DOI: https://doi.org/10.57233/ihcfs.046

ISBN: 978-978-68-07775

BOOK OF PROCEEDINGS

IHCFS – 2025 WEBSITE: fos.fugusau.edu.ng

$$t^* > 0 \begin{cases} u = \gamma \dfrac{\partial u^*}{\partial y^*}, \eta = T_\infty^* + \left(T_w^* - T_\infty^*\right)\epsilon e^{iwt}, \phi = C_\infty^* + \left(C_w^* - C_\infty^*\right)\epsilon e^{iwt} \; at \; \xi = 0 \\ u \to 0, \eta \to T_\infty^*, \phi \to C_\infty^* \quad as \; \xi \to \infty \end{cases} \tag{5}$$

where equations (1), (2), (3) and (4) refer to the continuity, momentum, energy and mass equations, respectively. Here $\dfrac{\partial v}{\partial y} = 0 \Rightarrow v = -v_c(1 + \varepsilon e^{nt})$.

The radiative heat flux term is simplified by making use of the Rosseland approximation as

$$q_r = -\frac{4\bar{\sigma}}{3k^*}\frac{\partial T^{*4}}{\partial y^*} \tag{6}$$

Here, $\bar{\sigma}$ is Stefan – Boltzmann constant and k* is the mean absorption coefficient. It is assumed that the temperature differences within the flow are sufficiently small so that T^{*4} can be expressed as a linear function of T^* after using Taylor's series to expand T^{*4} about the free stream temperature T_∞^* and neglecting higher – order terms. This results in the following approximation:

$$T^{*4} \cong 4T_\infty^{*3}T^* - 3T_\infty^{*4} \tag{7}$$

Using equations (6) and (7) in the last term of equation (3), we obtain:

$$\frac{\partial q_r}{\partial y^*} = -\frac{16\bar{\sigma}T_\infty^{*3}}{3k^*}\frac{\partial^2 T^*}{\partial y^{*2}} \tag{8}$$

Introducing (8) in the equation (3), the energy equation becomes:

$$\rho C_p\left[\frac{\partial T^*}{\partial t^*} + v\frac{\partial T^*}{\partial y^*}\right] = K_T\frac{\partial^2 T^*}{\partial y^{*2}} + \frac{16\bar{\sigma}T_\infty^{*3}}{3k^*}\frac{\partial^2 T^*}{\partial y^{*2}} - Q_0\left(T^* - T_\infty^*\right) \tag{9}$$

We define the following dimensionless quantities

$$\xi = \frac{u_c}{\upsilon}y^*, u = \frac{u^*}{u_c}, t = \frac{t^*u_c^2}{\upsilon}, \eta = \frac{T^* - T_\infty^*}{T_w^* - T_\infty^*}, \varphi = \frac{C^* - C_\infty^*}{C_w^* - C_\infty^*} \tag{10}$$

Substituting v, (9) and (10) into equations (2), (4) and (9), then, we have the following non – dimensional form of equations:

$$\frac{\partial u}{\partial t} - S(1 + \varepsilon e^{nt})\frac{\partial u}{\partial \xi} = \left(1 + \frac{1}{\beta}\right)\frac{\partial^2 u}{\partial \xi^2} - \left(M + \left(1 + \frac{1}{\beta}\right)\frac{1}{K}\right)u + Gr\eta + Gm\phi \tag{11}$$

$$\frac{\partial \eta}{\partial t} - S(1 + \varepsilon e^{nt})\frac{\partial \eta}{\partial \xi} = \frac{1}{\Pr}\left(\frac{3R + 4}{3R}\right)\frac{\partial^2 \eta}{\partial \xi^2} - H\eta \tag{12}$$

$$\frac{\partial \phi}{\partial t} - S(1 + \varepsilon e^{nt})\frac{\partial \phi}{\partial \xi} = \frac{1}{Sc}\frac{\partial^2 \phi}{\partial \xi^2} - Kc\phi \tag{13}$$

The corresponding initial and boundary conditions in non-dimensional form become:

$$u = u - \gamma\left(\frac{\partial u}{\partial \xi}\right), \eta = 1 + \varepsilon e^{iwt}, \phi = 1 + \varepsilon e^{iwt}, at \; \xi = 0$$

$$u \to 0, \eta \to 0, \phi \to 0 \text{ as } \xi \to 0 \tag{14}$$

DOI: https://doi.org/10.57233/ihcfs.046

ISBN: 978-978-68-07775

BOOK OF PROCEEDINGS

where $Sc=\frac{\upsilon}{D}, M=\frac{\delta\beta_0^2\upsilon}{\rho u_c^2}, Gr=\frac{\upsilon g\beta(T_w^*-T_w^*)}{u_0^3}, Gm=\frac{\upsilon\beta_1 g(C_w^*-C_\infty^*)}{u_0^3}, Kc=\frac{K^*\upsilon}{u_c^2},$

$S=\frac{v_c}{u_c}, K=\frac{K_p u_c^2}{\upsilon^2}, R=\frac{K_T k^*}{4\sigma T_\infty^{*3}}, H=\frac{Q_0\upsilon}{\rho C_p u_c^2}, \Pr=\frac{\mu C_p}{K_T},$

3.0 ANALYTICAL SOLUTIONS

The equations (11) to (13) are coupled non-linear PDEs in dimensionless form. To solve these equations subject to the boundary conditions (14), we assumed solution of the form:

$$\phi(\xi,t)=\phi_0(\xi)+\phi_1(\xi)\varepsilon e^{iwt}+(0)\varepsilon.... \quad (17)$$

$$u(\xi,t)=u_0(\xi)+u_1(\xi)\varepsilon e^{iwt}+(0)\varepsilon.... \quad (15)$$

$$\eta(\xi,t)=\eta_0(\xi)+\eta_1(\xi)\varepsilon e^{iwt}+(0)\varepsilon.... \quad (16)$$

Where expressions for u_0, u_1, η_0, η_1, ϕ_0, ϕ_1 are to be determined. Furthermore, other higher terms of ε will be neglected i.e. only the first two terms are considered.

Substituting equation (15) to (17) into (11) to (14), gives:

$$u_0: u_0^{''}+\frac{S}{\delta}u_0^{'}-\left(M+\frac{1}{K}\right)u_0=-\frac{Gr}{\delta}\eta_0-\frac{Gm}{\delta}\phi_0 \quad (18)$$

$$u_1: u_1^{''}+\frac{S}{\delta}u_1^{'}-\left(\frac{iw}{\delta}+\frac{M}{\delta}+\frac{1}{K}\right)u_1=-\frac{S}{\delta}u_0^{'}-\frac{Gr}{\delta}\eta_1-\frac{Gm}{\delta}\phi_1 \quad (19)$$

$$\eta_0: \eta_0^{''}+\frac{\Pr S}{\lambda}\eta_0^{'}-\frac{\Pr H}{\lambda}\eta_0=0 \quad (20)$$

$$\eta_1: \eta_1^{''}+\frac{\Pr S}{\lambda}\eta_1^{'}-\left(\frac{iw\Pr}{\lambda}+\frac{H\Pr}{\lambda}\right)\eta_1=-\frac{S\Pr}{\lambda}\eta_0^{'} \quad (21)$$

$$\phi_0: \phi_0^{''}+ScS\phi_0^{'}-ScKc\phi_0=0 \quad (22)$$

$$\phi_1: \phi_1^{''}+ScS\phi_1^{'}-(iwSc+ScKc)\phi_1=-ScS\phi_0^{'} \quad (23)$$

The boundary conditions are:

$$u_0-\gamma\left(\frac{\partial u_0}{\partial\xi}\right)=0, \eta_0=\eta_1=1, \phi_0=\phi_1=1 \text{ at } \xi=0 \quad (24)$$

$$u_0=u_1\to 0, \eta_0=\eta_1\to 0, \phi_0=\phi_1\to 0 \text{ as } \xi\to 0$$

Solving equations (18) to (23) subject to boundary conditions (24), the solutions for the velocity, temperature and concentration are as follows, respectively:

$$u(\xi,t)=N_{12}e^{-m_{10}\xi}+N_{13}e^{-m_6\xi}+N_{14}e^{-m_2\xi}+(N_{16}e^{-m_{12}\xi}+N_{17}e^{-m_{10}\xi}+N_{18}e^{-m_6\xi}+N_{19}e^{-m_2\xi}+N_{20}e^{-m_8\xi}$$
$$+N_{21}e^{-m_6\xi}+N_{22}e^{-m_4\xi}+N_{23}e^{-m_2\xi})\varepsilon e^{iwt}$$

(25)

$$\eta(\xi,t)=e^{-m_6\xi}+(N_9e^{-m_8\xi}+N_{10}e^{-m_6\xi})\varepsilon e^{iwt}$$

(26)

$$\varphi(\xi,t)=e^{-m_2\xi}+(N_4e^{-m_4\xi}+N_5e^{-m_2\xi})\varepsilon e^{iwt}$$

(27)

The Skin-friction, rate of heat and mass transfer, respectively at surface are as follows:

DOI: https://doi.org/10.57233/ihcfs.046

ISBN: 978-978-68-07775

BOOK OF PROCEEDINGS

IHCFS – 2025 WEBSITE: fos.fugusau.edu.ng

$$C_f = -\left(\frac{du}{d\xi}\right)_{\xi=0} = -m_{10}N_{12} - m_6N_{13} - m_2N_{14} - (m_{12}N_{16} + m_{10}N_{17} + m_2N_{18} + m_2N_{19} + m_8N_{20} + m_6N_{21} + m_4N_{22} + m_2N_{23})\varepsilon e^{iwt} \quad (28)$$

$$Nu = -\left(\frac{d\eta}{d\xi}\right)_{\xi=0} = -m_6 - (m_8N_9 + m_6N_{10})\varepsilon e^{iwt} \quad (29)$$

$$Sh = -\left(\frac{d\phi}{d\xi}\right)_{\xi=0} = -m_2 - (m_4N_4 + m_2N_5)\varepsilon e^{iwt} \quad (30)$$

4.0 RESULT AND DISCUSSION

Velocity slip effect on unsteady MHD natural convection flow of Casson fluid incorporating variable suction, thermal radiation and chemical reaction mechanisms has been solved analytically. The regular perturbation method was used to solve the governing equations of the flow field analytically to obtain the velocity, temperature and concentration fields. To have physical understanding of the problem computations were performed using MATLAB for varied physical parameters of interest.

4.1 Illustration for velocity profiles

Figure 1 depicts the effect of magnetic field parameter (M) on the velocity field. It is evident from the figure that an increase in the values of magnetic parameter reduces the velocity boundary layer. This is due to the fact that an increase in magnetic field develops the opposite force to the flow direction, which is called Lorentz force and it has the tendency to reduce the boundary layer thickness. Figure 2 illustrates the effect of permeability of porous medium (K) on fluid velocity. It is perceived from Fig. 2 that fluid velocity increases for increasing permeability parameter. From the flow configuration it is obvious that an increase in porosity of the medium assists the flow along the flow direction causing the fluid velocity to increase due to its orientation through the porous medium. Figures 3 and 4 depict the influence of thermal and concentration buoyancy forces (Gr and Gm) on fluid velocity. It is perceived seen that the fluid velocity increases on increasing values of Gr and Gm throughout the boundary layer region. Gr represents the relative strength of thermal buoyancy force to viscous force and Gm connotes the relative strength of concentration buoyancy force to viscous force. Therefore, Gr increases on increasing the strengths of thermal buoyancy force whereas Gm increases on increasing the strength of concentration buoyancy force. In this problem, natural convection flow induced due to thermal and concentration buoyancy forces; so, thermal and concentration buoyancy force tends to accelerate the fluid velocity throughout the boundary layer region which is clearly evident from Figures 3 and 4. Effect of Casson parameter (β) on velocity profile is clearly exhibited in Figure 5. It is observed that the fluid velocity increases close to the boundary of the wall with increasing values of (β). The effect of higher values of β is to increase the fluid velocity, and hence the boundary layer thickness increases. It can also be seen from Figure 5 that the momentum boundary layer thickness increases as β becomes signifiacant and hence induces a decrease in the absolute value of the velocity gradient at the surface. Figure 6 displays the velocity profiles for different values of suction parameter(S). The flux of the fluid in the boundary layer decreases when the intensity of the suction increases. The influence of Schmidt number (Sc) on the fluid velocity profiles are shown in Figure 7. It is noticed that, the fluid velocity profiles decrease on increasing the values of Sc. The Schmidt number embodies the ratio of the momentum to the mass diffusivity. The Schmidt number therefore quantifies the relative effectiveness of momentum to mass

DOI: https://doi.org/10.57233/ihcfs.046

ISBN: 978-978-68-07775

transport by diffusion in the hydrodynamic (velocity) boundary layers. The reductions in the velocity profiles are accompanied by simultaneous reductions in the velocity boundary layers. This behaviour is clear in Figure 7. Figure 8 presents the effect of chemical reaction parameter (Kc) on the fluid velocity. It is seen that, an increase in the chemical reaction parameter (Kc) leads to decrease in the thickness of the velocity boundary layer; this shows that diffusion rate can be tremendously altered by chemical reaction. It should be mentioned here that physically positive values of Kc implies destructive reaction and negative values of Kc implies generative reaction. We studied the case of a destructive chemical reaction. It is also noticed that concentration distributions decrease when the chemical reaction increase. Physically, for a destructive case, chemical reaction takes place with many disturbances. This, in turn, causes high molecular motion, which results in an increase in the transport phenomenon, thereby reducing the concentration distributions in the fluid flow. Figure 9 shows the effect of Prandtl number (Pr) on the fluid velocity profiles. Prandtl number embodies the ratio of viscous diffusion to thermal diffusion in the boundary layer regime. It also expresses the ratio of the product of specific heat capacity and dynamic viscosity, to the fluid thermal conductivity. When Pr is high, viscous diffusion rate exceeds thermal diffusion rate. On the basis of Figure 9, it is evident that the velocity curves drop as the Prandtl number Pr grows. The reasoning for this is because when the Prandtl number enhances, the thermal boundary layer width reduces since the fluid's thermal conductivity lowers as well. Figure 10 demonstrate the influence of thermal radiation parameter (R) on fluid velocity. It is clear from Figure 10 that, the thermal radiation causes decrease in the fluid's velocity. Physically, thermal radiation causes a fall in temperature of fluid medium and thereby causes a fall in kinetic energy of the fluid particles. This results in a corresponding decrease in the fluid velocity. Thus, Figure 10 is in excellent agreement with the laws of Physics. Figure 11 illustrates the influence of heat absorption parameter (H) on fluid velocity. It is evident from Figure 11 that as H increases, the pack value of fluid velocity tends to decrease. Physically, the presence of heat absorption coefficient has the tendency to reduce the fluid velocity. This cause the thermal buoyancy effects to decrease resulting in a net reduction in the fluid velocity.

DOI: https://doi.org/10.57233/ihcfs.046

ISBN: 978-978-68-07775

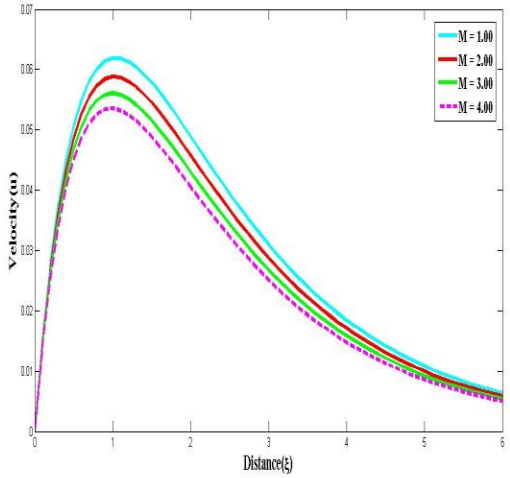

Figure 1: Velocity profile variations for Magnetic Parameter.

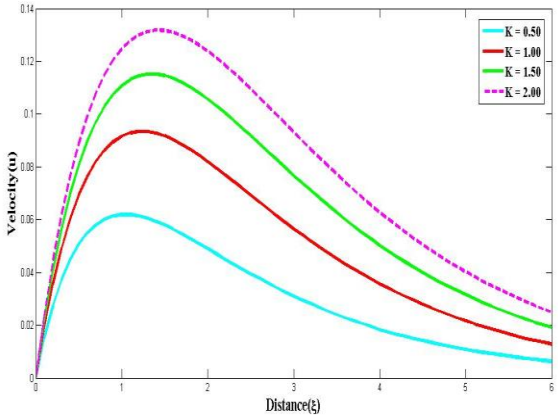

Figure 2: Velocity profile variations for permeability parameter.

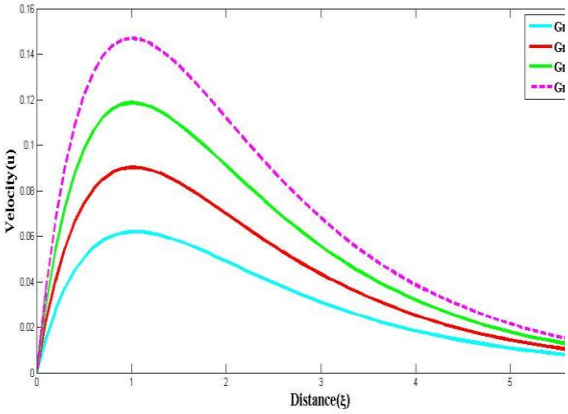

Figure 3: Velocity profile variations for thermal grashof number.

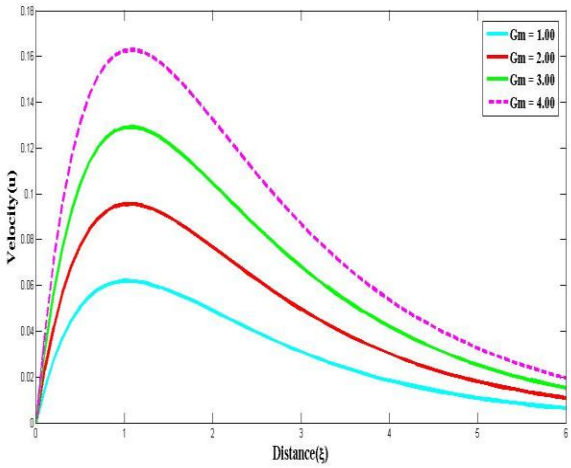

Figure 4: Velocity profile variations for mass Grashof Number.

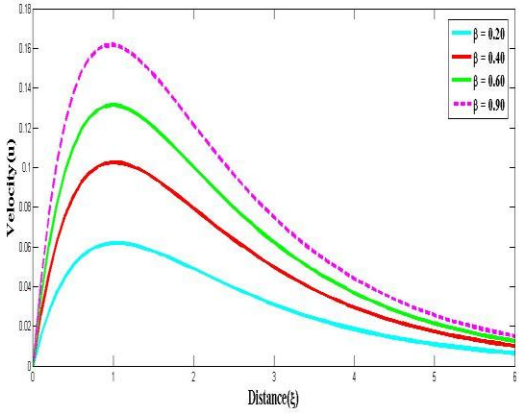

Figure 5: Velocity profile variations for Casson Parameter(β).

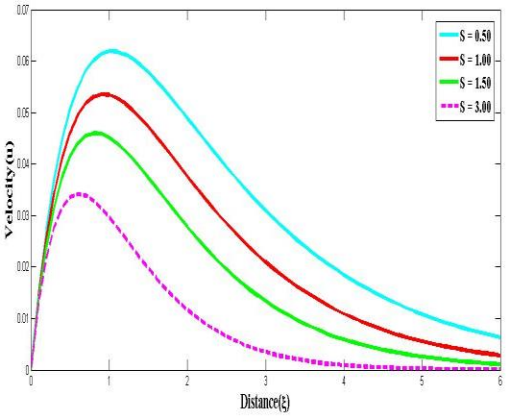

Figure 6: Velocity profile variations for Suction Parameter.

DOI: https://doi.org/10.57233/ihcfs.046

ISBN: 978-978-68-07775

BOOK OF PROCEEDINGS

IHCFS – 2025

WEBSITE: fos.fugusau.edu.ng

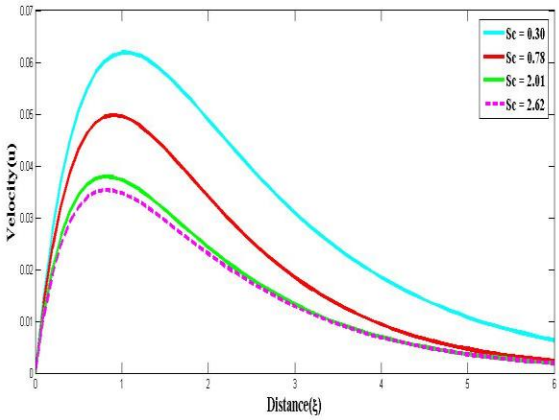

Figure 7: Velocity profile variations for Schmidt Number.

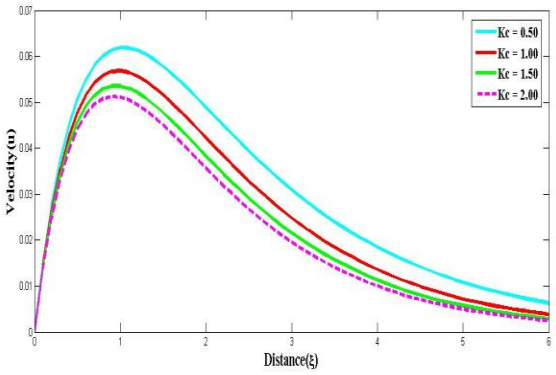

Figure 8: Velocity profile variations for Chemical Reaction Parameter.

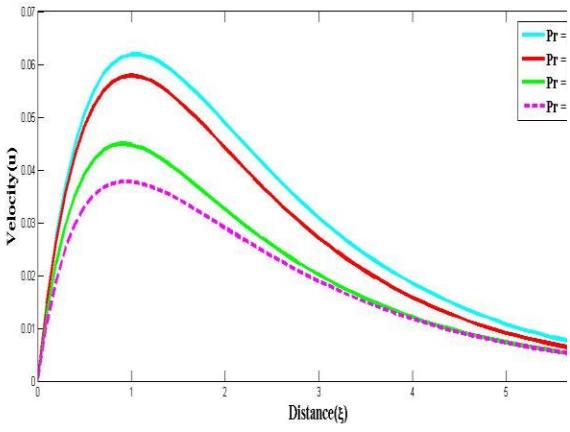

Figure 9: Velocity profile variations for Prandlt number.

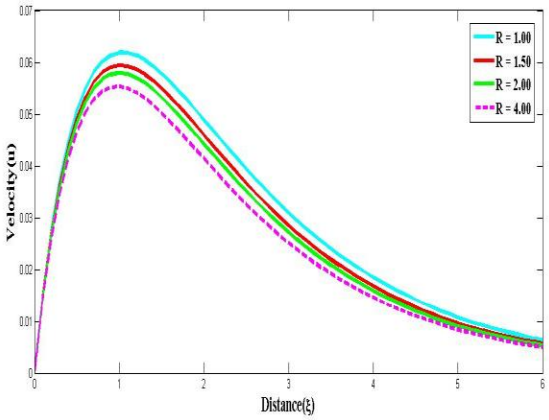

Figure 10: Velocity profile variations for Thermal Radiation Parameter.

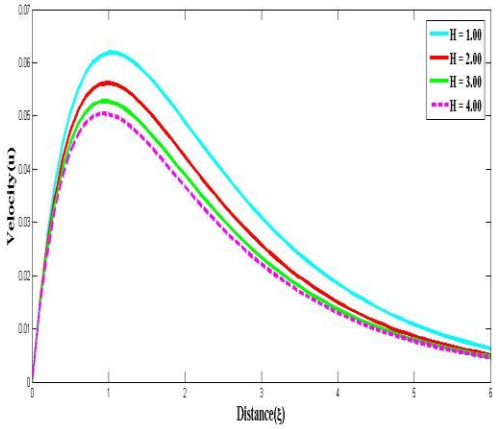

Figure 11: Velocity profile variations for Heat Absorption Parameter.

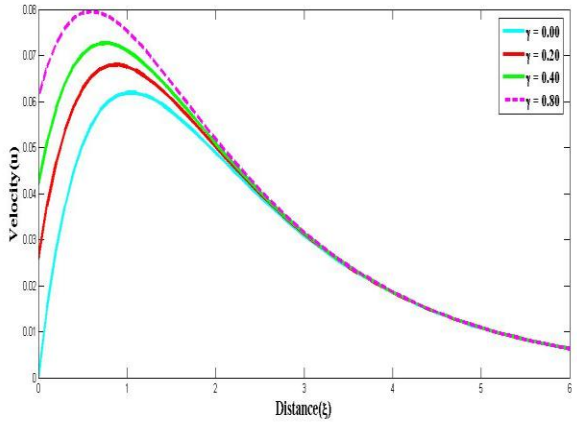

Figure 12: Velocity profile variations for Velocity Slip Parameter.

DOI: https://doi.org/10.57233/ihcfs.046

ISBN: 978-978-68-07775

BOOK OF PROCEEDINGS

4.2 Illustration for temperature profiles

Figure 13 presents the effect of Prandtl number (Pr) on the fluid velocity and temperature profiles. Prandtl number embodies the ratio of viscous diffusion to thermal diffusion in the boundary layer regime. It also expresses the ratio of the product of specific heat capacity and dynamic viscosity, to the fluid thermal conductivity. When Pr is high, viscous diffusion rate exceeds thermal diffusion rate. On the basis of Figure 13, it is found that the thermal curves drops as the Prandtl number (Pr) grows. The reasoning for this is because when the Prandtl number enhances, the thermal boundary layer width reduces since the fluid's thermal conductivity become lower as well. Figure 14, demonstrate the influence of thermal radiation parameter (R) on fluid temperature. It is evident from Figure 14 that, the thermal radiation leads to decrease the fluid temperature. Physically, thermal radiation causes a fall in temperature of fluid medium and thereby causes a fall in kinetic energy of the fluid particles. Thus, Figure 14 is in excellent agreement with the laws of Physics. Figure 15, illustrates the influence of heat absorption parameter (H) on fluid temperature. It is obvious that, as H increases the pack value fluid temperature tends to decrease. Physically, the presence of heat absorption coefficient has the tendency to reduce the fluid temperature. This cause the thermal buoyancy effects to decrease resulting in a net reduction in the fluid temperature. Figure 16 shows the effect of suction on the thermal boundary layer. It is observed that the temperature of the fluid reduces as suction parameter becomes significant.

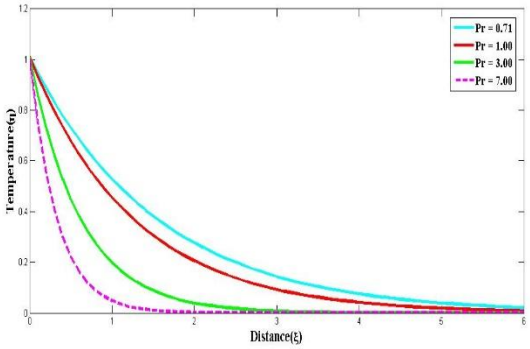

Figure 13: Temperature profile variations for Prandlt number.

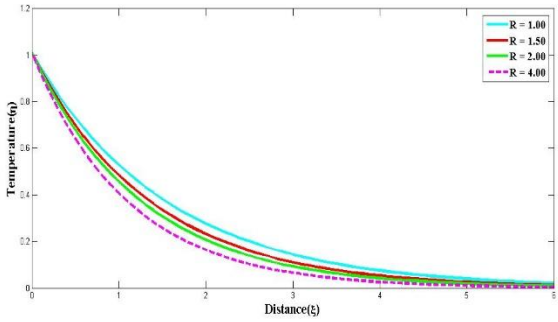

Figure 14: Temperature profile variations for Thermal Radiation parameter.

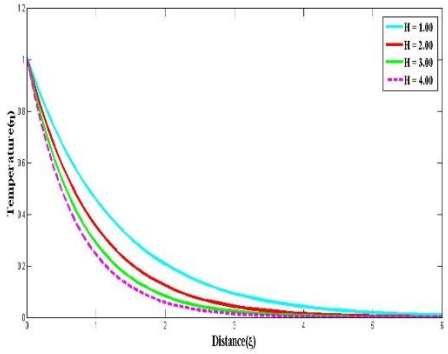

Figure 15: Temperature profile variations for Heat absorption parameter.

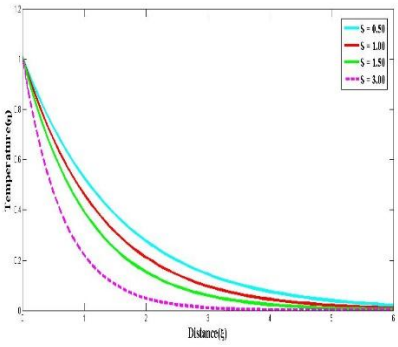

Figure 16: Temperature profile variations for Suction parameter.

DOI: https://doi.org/10.57233/ihcfs.046

ISBN: 978-978-68-07775

BOOK OF PROCEEDINGS

4.3 Illustration for concentration profiles

The influence of Schmidt number (Sc) on the fluid concentration profiles are depicted in Figure 17, respectively. It is noticed that, the fluid concentration profiles decreases on increasing the values of Sc. The Schmidt number embodies the ratio of the momentum to the mass diffusivity. The Schmidt number therefore quantifies the relative effectiveness of momentum to mass transport by diffusion in the concentration (species) boundary layers. As the Schmidt number increases the concentration decreases. This cause the concentration buoyancy effects to decrease yielding a reduction in the fluid concentration. The reductions in the concentration profiles are accompanied by simultaneous reductions in the concentration boundary layers. This behavior is clear from Figure 17. Figure 18 illustrates the effect of chemical reaction parameter (Kc) on the fluid concentration. As can be seen, an increase in the chemical reaction parameter (Kc) leads to decrease in the thickness of the concentration boundary layer; this shows that diffusion rate can be tremendously altered by chemical reaction. It should be mentioned here that physically positive values of (Kc) implies destructive reaction and negative values of (Kc) implies generative reaction. We studied the case of a destructive chemical reaction. It is noticed that concentration distributions decrease when the chemical reaction increase. Physically, for a destructive case, chemical reaction takes place with many disturbances. This, in turn, causes high molecular motion, which results in an increase in the transport phenomenon, thereby reducing the concentration distributions in the fluid flow. Figure 19 shows the effect of suction parameter on concentration profile. It is seen that the fluid's concentration falls as suction parameter is increased.

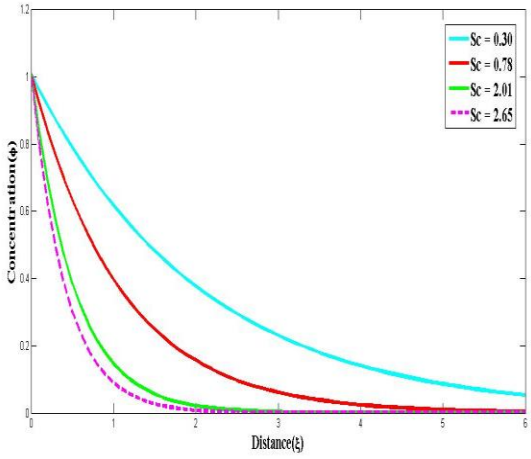

Figure 17: Concentration profile variations for Schmidt number.

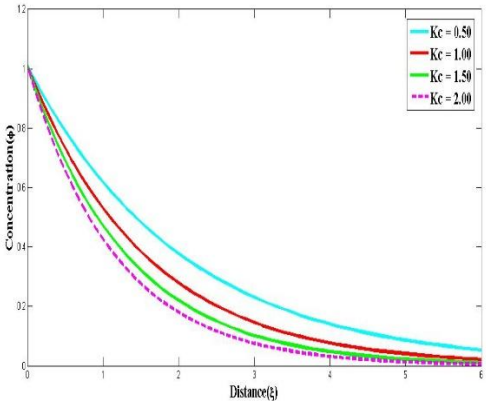

Figure 18: Concentration profile variations for chemical reaction parameter.

DOI: https://doi.org/10.57233/ihcfs.046

ISBN: 978-978-68-07775

BOOK OF PROCEEDINGS

IHCFS – 2025

WEBSITE: fos.fugusau.edu.ng

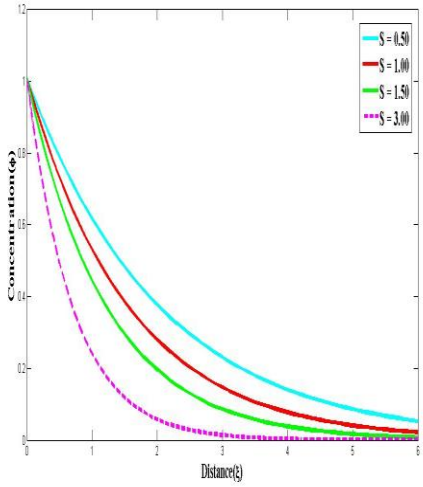

Figure 19: Concentration profile variations for Suction parameter.

5.0 CONCLUSION

We examined the effects of velocity slip, variable suction, thermal radiation on Casson fluid flow. The differential equations governing the flow of the fluid were solved by perturbation method to obtain the velocity, temperature and concentration fields, respectively. Computations were performed for physical parameters of interest to show how these parameters affect the velocity, temperature and concentration profiles. The main conclusion are as follows:

a. The velocity profile across the surface reduces as M, S, Pr, R, H, Sc, and Kc parameters rise, but the velocity improves as Gr, Gm, K, β, and γ become significant.
b. The temperature profile across the surface reduces as Pr, R, H, and S parameters rises.
c. There are downward trends in the concentration pattern for increased values of Sc, Kc, S.

REFERENCES

Agarwalla S., and Ahmed N. (2018). MHD mass transfer flow past an inclined plate with variable temperature and plate velocity embedded in a porous medium, heat transfer. *Asian Research*. 47(1), 27-41. https://doi.org/10.1002/htj.21288.

Akbar, N., Muhammad, S. H., and Ullah Khan, R. (2022). Numerical solution of casson fluid flow under viscous dissipation and radiation phenomenon. *Journal of Applied Mathematics and Physics*. 10, Pp 475-490. https://www.scirp.org/journal/jamp. ISSN Print: 23274352.

Gireesha B.J. and Sindhu S. (2020). MHD natural convection flow of Casson fluid in an annular microchannel containing porous medium with heat generation/absorption. *Nonlinear Engineering*. 9, 223–232. https://doi.org/10.1515/nleng-2020-0010.

Hayat, T., Qayyum, A. and Alsaedi, A. (2014) Effects of heat and mass transfer

in flow along a vertical stretching cylinder with slip conditions. *Eur Phys J Plus*. 129(4),63.

Ibrahim, F. S., Elaiw, A.M. and A. A, and Bakr, A. A., (2008). Effect of the chemical reaction and radiation absorption on the unsteady MHD free convection flow past a semi-infinite vertical permeable moving plate with heat source and suction. *Communications in Non-linear Science and Numerical Simulation.* 13, 1056-1066. https://doi.org/10.1016/j.cnsns.2006.09.007.

Joshna, N., Seshagiri, Rao Y.V. and Saroja S. (2022). Role of chemical reaction on heat and mass transfer in a permeable vertical plate. *Journal of Positive School Psychology* (6) 5, Pp: 1865-1873. http://journalppw.com

Kadeethum, T., Ballarin, F., Choi, Y., O'Malley, D., Yoon, H and Bouklas, N. (2022). Non-intrusive reduced order modeling of natural convection in porous media using convolutional autoencoders: comparison with linear subspace techniques. *Advances in Water Resource.* 160, 104098.

Kumar, A. D. (2020). In presence of thermal radiation through porous medium unsteady mhd casson fluid flow past an accelerated vertical plate. *International Journal of Statistics and Applied Mathematics.* 5(4): 213-214. http://www.mathsjournal.com. ISSN: 2456-1452.

Kumar, S. and Singh, A. (2023). Application of the Casson fluid model in food processing: ketchup and toothpaste rheology. *Food Science & Nutrition*. 11(4). 2351-2360. DOI: https://doi.org/10.1002/fsn3.2877.

Mahmood, Z., Ur Rehman, M., Khan, U., Ali, B., & Haque Siddiqui, M. I. (2025). Enhanced transport phenomena in Casson fluid flow over radiative moving surface: Influence of velocity and thermal slip conditions with mixed convection and chemical reaction. *Modern Physics Letters B*, *39*(01), .https://doi.org/10.1142/S0217984924503834

Manthramurthy, P., & Vempati, S. R. (2025). Significance of multiple slips and thermal radiation on heat and mass transfer in MHD Casson nanofluid flow over an exponentially stretching porous sheet with non-uniform heat source and sink. *Multiscale and Multidisciplinary Modeling, Experiments and Design*, *8*(3), 1-18. https://doi.org/10.1007/s41939-025-00743-0

Mishra, A. and Kumar, M. (2020). Velocity and thermal slip effects on MHD nanofluid flow past a stretching cylinder with viscous dissipation and Joule heating. *Journal of Springer Nature Applied Sciences.* 2,1350. https://doi.org/10.1007/s42452-020-3156-7.

Mukhopadhyay, S. (2013) MHD boundary layer slip flow along a stretching cylinder. *Ain Shams Eng J*. 4(2),317–324 8.

Omokhuale E., and Jabaka M. L. (2019). Magnetohydrodynamic Casson fluid flow over an infinite vertical plate with chemical reaction and heat generation. *American Journal of Computational Mathematics*, 9, 187 – 200. https://doi.10.4236/ajcm.2019.93014

Omokhuale, E. and Jabaka, M. L. (2020a). Magnetohydrodynamic Casson fluid flow past a vertical plate in the presence of thermal conductivity and chemical absorption. *International Journal of Science for Global Sustainability, IJSGS*, 6(2), 82 – 90.

Omokhuale, E. and Jabaka, M. L. (2020b). Effect of radiation on heat and mass transfer magnetohydrodynamic Casson

fluid flow in a vertical channel. *Caliphate Journal of Science and Technology* (CaJoST), 2020, 2, 73 – 80.

Prakash, J., Selvaraj, A., Ragupathi, P., Al-Mdallal, Q. M., & Saranya, S. (2025). Thermal and radiative effects on unsteady mhd flow of casson fluid past a rotating porous medium with variable mass diffusion. *Case Studies in Thermal Engineering*. https://doi.org/10.1016/j.csite.2025.105865

Ragulkumar, E., Sambath, P., Suresh, K., Balasubramanian, S., and Chamkhad, A. J. (2023). Soret–Dufour mass transfer effects on radiative chemically dissipative MHD plain convective water nanofluid (Al2O3, Cu, Ag, & TiO2) flow across a temperature-controlled upright cone surface with heat blow/suction. *An International Journal of Computation and Methodology.* https://doi.org/10.1080/10407782.2023.2261626.

Rajakumar, K. V.B., Pavan, V. S. R. Rayaprolu, K., Balamurugan, K. S. and Kumar V. B. (2020). Unsteady MHD Casson dissipative fluid flow past a semi-infinite vertical porous plate with radiation absorption and chemical reaction in presence of heat generation. Mathematical Modelling of Engineering Problems. 7(1), pp. 160-172. https://doi.org/10.18280/mmep.070120.

Wang, C.Y. and Ng CO (2011) Slip flow due to a stretching cylinder. *International Journal of Non-Linear Mech*. 46(9):1191–1194 7.

DOI: https://doi.org/10.57233/ihcfs.046

ISBN: 978-978-68-07775

BOOK OF PROCEEDINGS

Appendix

$$c_1 = \sqrt{\frac{(ScS)^2 + 4(ScKc)}{4}}, \quad c_2 = \sqrt{\frac{(ScS)^2 + 4(iwSc + ScKc)}{4}}, \; m_2 = \frac{ScS}{2} + c_1, \; m_4 = \frac{ScS}{2} + c_2$$

$$N_4 = 1 - N_5, \; N_5 = \frac{-ScSm_2}{m_2^2 - ScSm_2 - (iwSc + ScKc)}, \; \phi_0(\xi) = e^{-m_2\xi}, \; \phi_1(\xi) = N_4 e^{-m_4\xi} + N_5 e^{-m_2\xi}$$

$$\lambda = \left(\frac{3R+4}{3R}\right), \; c_3 = \sqrt{\frac{\left(\frac{\Pr S}{\lambda}\right)^2 + 4\left(\frac{\Pr H}{\lambda}\right)}{4}}, \; c_4 = \sqrt{\frac{\left(\frac{\Pr S}{\lambda}\right)^2 + 4\left(\frac{\Pr}{\lambda}(H + iw)\right)}{4}} \; m_6 = \frac{2\Pr S}{\lambda} + c_3$$

$$m_8 = \frac{2\Pr S}{\lambda} + c_4, \; N_9 = I - N_{10}, \; N_{10} = \frac{\frac{S\Pr m_6}{\lambda}}{\left(m_6^2 - \frac{S\Pr}{\lambda}m_6 - \left(\frac{iw\Pr}{\lambda} + \frac{H\Pr}{\lambda}\right)\right)}, \; \eta_0(\xi) = e^{-m_6\xi}$$

$$\eta_1(\xi) = N_9 e^{-m_8\xi} + N_{10} e^{-m_6\xi}, \; \delta = \left(\frac{1}{\beta} + 1\right), \; c_5 = \sqrt{\frac{\left(\frac{S}{\delta}\right)^2 + 4\left(\frac{M}{\delta} + \frac{1}{K}\right)}{4}}$$

$$c_6 = \sqrt{\frac{\left(\frac{S}{\delta}\right)^2 + 4\left(\frac{M}{\delta} + \frac{1}{K} + \frac{iw}{\delta}\right)}{4}}, \; m_{10} = \frac{2S}{\delta} + c_5, \; m_{12} = \frac{2S}{\delta} + c_6$$

$$N_{13} = \frac{\frac{-Gr}{\delta}}{\left(m_6^2 - \frac{S}{\delta}m_6 - \left(\frac{M}{\delta} + \frac{1}{K}\right)\right)}, \; N_{14} = \frac{\frac{-Gm}{\delta}}{\left(m_2^2 - \frac{S}{\delta}m_2 - \left(\frac{M}{\delta} + \frac{1}{K}\right)\right)}$$

$$N_{12} = \frac{-N_{13}(1 + \gamma m_6) - N_{14}(1 + \gamma m_2)}{(1 + \gamma m_{10})}, \; N_{17} = \frac{\frac{Sm_{10}N_{12}}{\delta}}{\left(m_{10}^2 - \frac{S}{\delta}m_{10} - \left(\frac{iw}{\delta} + \frac{M}{\delta} + \frac{1}{K}\right)\right)}$$

$$N_{18} = \frac{\frac{Sm_6N_{13}}{\delta}}{\left(m_6^2 - \frac{S}{\delta}m_6 - \left(\frac{iw}{\delta} + \frac{M}{\delta} + \frac{1}{K}\right)\right)}, \; N_{19} = \frac{\frac{Sm_2N_{14}}{\delta}}{\left(m_2^2 - \frac{S}{\delta}m_2 - \left(\frac{iw}{\delta} + \frac{M}{\delta} + \frac{1}{K}\right)\right)}$$

$$N_{20} = \frac{\frac{-GrN_9}{\delta}}{\left(m_8^2 - \frac{S}{\delta}m_8 - \left(\frac{iw}{\delta} + \frac{M}{\delta} + \frac{1}{K}\right)\right)}, \; N_{21} = \frac{\frac{-GrN_{10}}{\delta}}{\left(m_6^2 - \frac{S}{\delta}m_6 - \left(\frac{iw}{\delta} + \frac{M}{\delta} + \frac{1}{K}\right)\right)}$$

DOI: https://doi.org/10.57233/ihcfs.046

ISBN: 978-978-68-07775

BOOK OF PROCEEDINGS

$$N_{22} = \frac{\frac{-GmN_4}{\delta}}{\left(m_4^2 - \frac{S}{\delta}m_4 - \left(\frac{iw}{\delta} + \frac{M}{\delta} + \frac{1}{K}\right)\right)},\ N_{23} = \frac{\frac{-GmN_5}{\delta}}{\left(m_2^2 - \frac{S}{\delta}m_2 - \left(\frac{iw}{\delta} + \frac{M}{\delta} + \frac{1}{K}\right)\right)}$$

$$N_{16} = \frac{-N_{17}(1+\gamma m_{10}) - N_{18}(1+\gamma m_6) - N_{19}(1+\gamma m_2) - N_{20}(1+\gamma m_8) - N_{21}(1+\gamma m_6) - N_{22}(1+\gamma m_4) - N_{23}(1+\gamma m_2)}{(1+\gamma m_{12})}$$

$$U_0(\xi) = N_{12}e^{-m_{10}\xi} + N_{13}e^{-m_6\xi} + N_{14}e^{-m_2\xi}$$

$$U_1(\xi) = N_{16}e^{-m_{12}\xi} + N_{17}e^{-m_{10}\xi} + N_{18}e^{-m_6\xi} + N_{19}e^{-m_2\xi} + N_{20}e^{-m_8\xi} + N_{21}e^{-m_6\xi} + N_{22}e^{-m_4\xi} + N_{23}e^{-m_2\xi}$$